Hindawi Publishing Corporation
Journal of Nanomaterials
Volume 2015, Article ID 850147, 15 pages
http://dx.doi.org/10.1155/2015/850147

Review Article

SnO_2-Based Nanomaterials: Synthesis and Application in Lithium-Ion Batteries and Supercapacitors

Qinqin Zhao, Lisha Ma, Qiang Zhang, Chenggang Wang, and Xijin Xu

School of Physics and Technology, University of Jinan, 336 Nanxin Zhuang West Road, Jinan, Shandong 250022, China

Correspondence should be addressed to Xijin Xu; sps_xuxj@ujn.edu.cn

Received 8 August 2014; Accepted 24 September 2014

Academic Editor: Chuanfei Guo

Copyright © 2015 Qinqin Zhao et al. This is an open access article distributed under the Creative Commons Attribution License, which permits unrestricted use, distribution, and reproduction in any medium, provided the original work is properly cited.

Tin dioxide (SnO_2) is an important n-type wide-bandgap semiconductor, and SnO_2-based nanostructures are presenting themselves as one of the most important classes due to their various tunable physicochemical properties. In this paper, we firstly outline the syntheses of phase-pure SnO_2 hierarchical structures with different morphologies such as nanorods, nanosheets, and nanospheres, as well as their modifications by doping and compositing with other materials. Then, we reviewed the design of SnO_2-based nanostructures with improved performance in the areas of lithium-ion batteries (LIBs) and supercapacitors.

1. Introduction

As one of the most important classes of materials, metal oxide semiconductor nanomaterials present themselves in various areas of science and technology, due to their shape- and size-dependent physical and chemical properties [1, 2]. Among various metal oxide nanomaterials, SnO_2 has become the foremost one, because of its wide applications in lithium batteries [3–6], supercapacitors [7–10], gas sensors [11, 12], and catalysis [13, 14]. Recently, reports on the applications of SnO_2 nanostructures mainly depend on their morphologies and structural features. Thus, considerable efforts have been devoted to synthesizing SnO_2 nanostructures with different morphologies, such as nanorods [15–17], nanowires [18–20], nanotubes [11], nanosheets [2, 21], and 3D nanospheres self-assembled from these low-dimensional nanostructures via interactions such as van der Waals forces, hydrogen, and covalent bonding [3, 22–24].

Various methods have been adopted for the preparation of nanoscaled SnO_2 nanostructures, such as hydrothermal route and template method. However, because the performance enhancement to meet the increasing requirements is still to be a challenge, then many researchers have established various ways to improve the performance of SnO_2-based materials, including doping [25, 26], synthesis of stannate nanomaterials [27], and constructing the heterojunctions [28]. In this respect, development of suitable synthetic strategies has become crucial to achieve the desired properties.

In this review, we outline the synthetic strategies of phase-pure SnO_2 hierarchical structures and the approaches to enhance the performance. The applications of hierarchical SnO_2-based nanostructures in lithium-ion batteries and supercapacitors are also reviewed. By focusing on the hierarchical SnO_2-based nanostructures, we hope to provide a better understanding on their physicochemical properties and the design principles when used in energy conversion and energy storage and further explore the new possibilities to advance the future research.

2. SnO_2-Based Nanomaterials

2.1. Phase-Pure SnO_2 Nanostructures. Many researchers have devoted their efforts to manipulate the structures and morphologies of SnO_2 in order to improve the performances and widen their applications. Two kinds of synthesis strategies have generally been explored as follows.

(1) Hydrothermal Method. Hydrothermal method has been paid much attention, due to its simplicity, low cost, high efficiency, and convenient manipulation combined with flexible control over the sizes and morphologies of the resulting nanostructures [9, 11, 17, 23, 24], in which aqueous solution

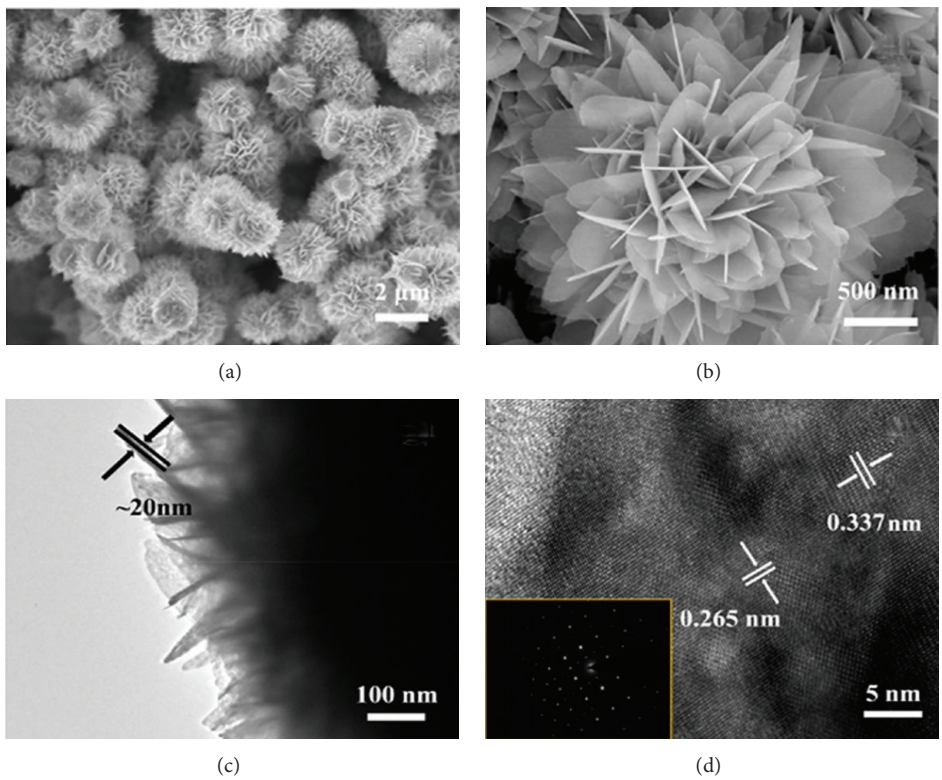

Figure 1: (a)-(b) FESEM images, (c) low-magnification TEM image, and (d) high-resolution TEM (HRTEM) image of the prepared hierarchical SnO_2 nanostructures. Inset in d exhibits the typical corresponding SAED pattern adapted from [2] with permission.

is used as the reaction medium, to create a high temperature and high pressure reaction environment by heating the reaction vessel to a certain temperature. In 2004, Cheng et al. [16] synthesized single-crystalline SnO_2 nanorods with diameter of about 5 nm and length of about 20 nm. Furthermore, many researchers developed the method and synthesized different SnO_2 architectures by adjusting the precursors and experimental conditions [2, 11, 17]. For example, SnO_2 hollow microspheres composed of SnO_2 nanoparticles have been synthesized [29]. Recently, Liu et al. [2] developed a facile approach to fabricate hierarchical SnO_2 nanosheets, using $SnCl_2{\cdot}2H_2O$ as tin source and sodium citrate as controlling agents. The ultrathin nanosheets with a thickness of about 20 nm are shown in Figures 1(a) and 1(b), which corresponds to the TEM image of Figure 1(c). The HRTEM image (Figure 1(d)) exhibits the well-defined lattice fringes combined with the SAED pattern. Their growth mechanism is generally summarized in Figure 2 [2, 30]. First of all, SnO_2 nanocrystals were formed due to the hydrolysis of $SnCl_2$, whereas in the second step, the grown small SnO_2 nanoparticles are further assembled with each other to form nanosheets because of the "oriented attachment" growth process. Subsequently, the fast oriental attachment of the SnO_2 nanoparticles results in the formation of SnO_2 nanosheets. Moreover, the new formed particles would spontaneously "land" on the as-formed sheets and further grow to another sheet, which led to the formation of flower-like SnO_2 architectures.

(2) Template Method. Template-based methods offer many advantages, including simplicity, low cost, and narrow size distribution [11]. However, there are some limitations. For example, the post treatment process of the templates always damages the nanoarchitectures, and it is difficult to remove the template and limit the ability to produce large-scaled nanomaterials. Generally, templates such as silica nanorods [31], MoO_3 nanorods [32], and carbon nanotubes [33] can be removed through calcination at high temperature (e.g., to remove carbon or polystyrene spheres), or chemical dissolution (e.g., use of hydrofluoric acid to remove silica templates), which may result in collapse of some fraction of the hollow structures [34, 35]. Therefore, it is highly desirable to develop new strategies for synthesizing hollow SnO_2 nanostructures. Zhang et al. [11] developed a reactive-template method to fabricate porous SnO_2 nanotubes using MnO_2 nanorods as the sacrificial template. The overall synthesis procedure is illustrated in Figure 3, which is based on the redox chemistry between reductive Sn^{2+} and oxidative MnO_2 in an acidic environment. Chemical reactions for the formation of SnO_2 nanotubes included in a basic aqueous solution are shown in (1)–(3):

$$MnO_2 + 4H^+ + 2e^{-1} \longrightarrow Mn^{2+} + 2H_2O \quad (1)$$

$$Sn^{4+} + 2e^{-1} \longrightarrow Sn^{2+} \quad (2)$$

$$MnO_2 + Sn^{2+} + 2H_2O \longrightarrow Mn^{2+} + Sn(OH)_4. \quad (3)$$

When the MnO_2 nanorods are completely dissolved because of reduction, then the $Sn(OH)_4$ nanotubes with a hollow interior are eventually formed. Finally, porous SnO_2

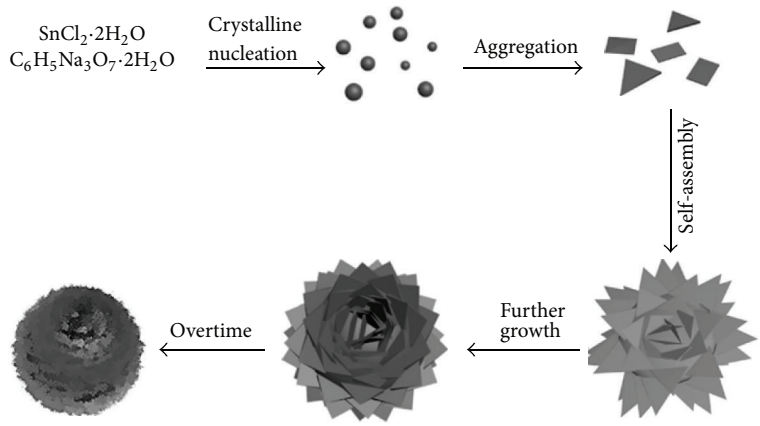

Figure 2: Schematic for the possible growth of the as-synthesized hierarchical SnO_2 nanostructures adapted from [2] with permission.

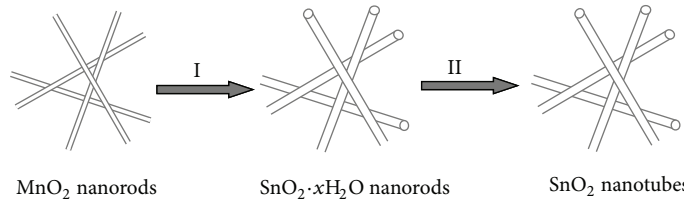

Figure 3: Synthesis process for SnO_2 nanotubes via a reactive-template strategy adapted from [11] with permission.

nanotubes were obtained by annealing the product at 500°C for 2 h ((4)-(5)):

$$\mathrm{Sn(OH)_4} \longrightarrow \mathrm{SnO_2 \cdot \mathit{x}H_2O} + (2 - \mathit{x})\,\mathrm{H_2O} \quad (4)$$

$$\mathrm{SnO_2 \cdot \mathit{x}H_2O} \longrightarrow \mathrm{SnO_2} + 2\mathrm{H_2O} \quad (5)$$

The morphologies of the MnO_2 nanorods and the as-prepared SnO_2 nanotubes (Figures 4(a), 4(b), and 4(c)) exhibit their 1D structure. The SnO_2 nanotubes show a rough surface because the tube walls are composed of many nanoparticles with a size in the range of 5–15 nm (Figures 4(d) and 4(e)). The hollow porous structure of the nanotubes is also visible, as indicated by the dashed lines in Figures 4(d) and 4(e). The pore-size distribution (inset of Figure 4(f)) calculated using the Barrett-Joyner-Halenda (BJH) method for both the adsorption and desorption branches of the isotherm indicates that most of the pores have a diameter in the range of 2–6 nm. Such porous structure leads to a Brunauer-Emmett-Teller (BET) specific surface area of 66.1 m^2/g.

Wang et al. [36] fabricated SnO_2nanorods that consisted of SnO_2 hollow microspheres via the soft template relying on the use of $(CH_2)_6N_4$ and demonstrated that it is a nontoxic, water-soluble method to prepare the hollow structure under the hydrothermal treatment.

(3) Other Synthesis Methods. Besides the above-mentioned methods, there are many other approaches for the fabrication of SnO_2-based nanostructures. Spray pyrolysis is a process for preparing particles or films by forming droplets from a precursor solution and then evaporating and decomposing them in a reactor. This process has proven to be quite useful for the preparation of various nanostructure and composite particles, as is shown in Figure 5, with many reports onto the effect of the main variables on particle formation [37]. Hong et al. [38] prepared Pd-loaded double-shelled SnO_2 yolk-shell spheres by one-step spray pyrolysis. Patil et al. [39] synthesized high-purity nanostructured SnO_2 powders through spray pyrolysis. Ju et al. [40] reported the use of spray pyrolysis to produce SnO_2 powders with uniform morphology and narrow size distribution. In addition, others method are also used to synthesize SnO_2-based nanostructures. Yan et al. [41] synthesized the hierarchical SnO_2 hollow spheres by two layers of tetragonal prism nanorod arrays, formed on the surface of self-generated NO bubbles in the aqueous solution. This method is promising in the design of the hollow structures without further heat treatment. Dai et al. [18] synthesized SnO_2 nanowires, sandwiched nanoribbons, and nanotubes by high temperature thermal oxide method. Chen et al. [15] reported that SnO_2 nanorod arrays were synthesized in a ternary solvent system comprising acetic acid, ethanol, and water using $SnCl_4$ as the Sn source and NaBr as the additive. The growth of SnO_2 crystals was carefully controlled in the mixed solvents, leading to the exclusively heterogeneous nucleation on a substrate and finally the mesocrystalline nanorod arrays were obtained. Most of the above methods are illustrated in Table 1.

2.2. Doped Hierarchical SnO_2 Nanostructures. Doping of oxide nanomaterials is a general approach to tailor their electrical and optical properties. Thus, many efforts have been carried out to improve the performance of the materials

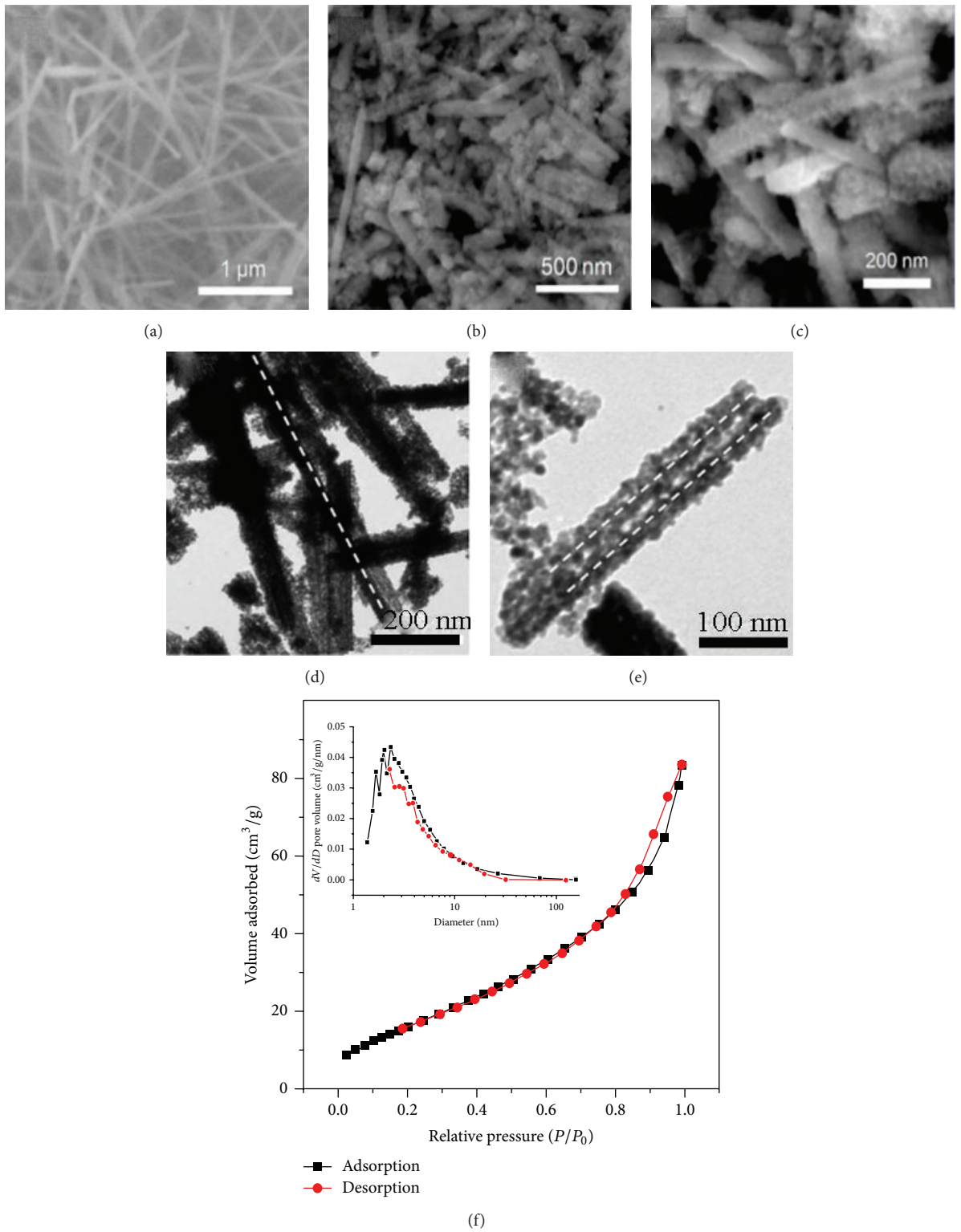

FIGURE 4: SEM images of (a) MnO_2 nanorods and ((b), (c)) SnO_2 nanotubes. ((d), (e)) TEM images of SnO_2 nanotubes. (f) N_2 adsorption-desorption isotherm with the BJH pore-size distribution in the inset, adapted from [11] with permission.

Table 1: Summary of various methods for SnO_2-based nanostructure synthesis.

Structure type	Method	Matrix	Growth reagent	Growth condition	Reference
SnO_2 nanosheets	Hydrothermal method	In solution	$SnCl_2{\cdot}2H_2O$, $C_6H_5Na_3O{\cdot}2H_2O$ ethanol, water	Autoclave 180°C, 8 h	[2]
3D SnO_2 nanoflowers	Hydrothermal method	Ti foil	$SnCl_4{\cdot}5H_2O$, NaOH, water	Autoclave 200°C (2, 4, 8, 16 h)	[9]
Zn-doped SnO_2 nanorods	Hydrothermal method	In solution	$SnCl_4{\cdot}5H_2O$, $ZnCl_2$, NaOH, ethanol, water	Autoclave 200°C, 24 h	[14]
Single-crystalline SnO_2 nanorods	Hydrothermal method	In solution	$SnCl_4{\cdot}5H_2O$, alcohol, water	Autoclave 150°C, 24 h	[16]
SnO_2 hollow microspheres	Hydrothermal method	In solution	$SnCl_4{\cdot}5H_2O$, carbamide, water	Autoclave 160°C, 16 h	[29]
Porous SnO_2 nanotubes	Template method	In solution	$MnSO_4{\cdot}H_2O$, $SnCl_2{\cdot}2H_2O$, HCL	Autoclave 160°C, 12 h	[11]
SnO_2 hollow microspheres	Template method	In solution	$SnCl_2$, H_2O_2, NaOH, $(CH_2)_6N_4$	Autoclave 200°C, 30 h	[36]
Pd-Loaded SnO_2 Yolk-Shell nanostructures	Spray pyrolysis	Spray solution	C_2O_4Sn, $Pd(NO_3)_2{\cdot}xH_2O$, $C_{12}H_{22}O_{11}$, HNO_3	Air flow rate 10 $Lmin^{-1}$, 1000°C	[38]
SnO_2 nanoparticles	Spray pyrolysis	Spray solution	$SnCl_4{\cdot}5H_2O$	Air flow rate 17 kg/m^2, 673 K and 1073 K	[39]
SnO_2 powders	Spray pyrolysis	Spray solution	$SnCl_4{\cdot}5H_2O$, citric acid, ethylene glycols	Gas flow rate 40 L/min, 900°C	[40]
Tin Oxide nanowires, nanoribbons, and nanotubes	High temperature thermal oxide method	Gas	Sn foil + SnO-layered N_2 flow gas	Lindberg blue tube furnace configuration 1050–1150°C	[18]

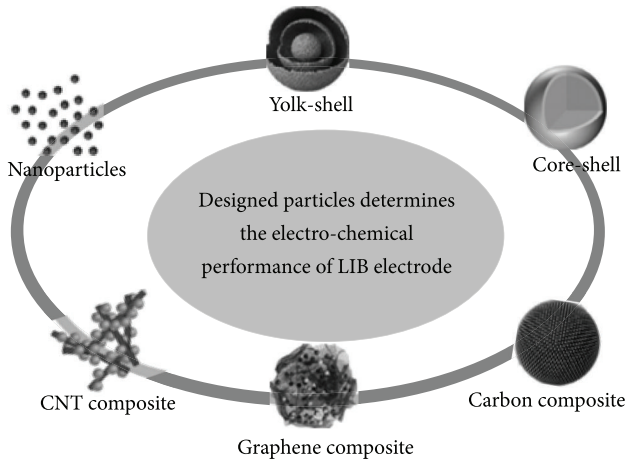

Figure 5: Various nanostructure and composite particles prepared by spray pyrolysis adapted from [37] with permission.

by doping other elements. For example, Yin and Guo [42] prepared Fe-doped SnO_2 gas sensor for CO detection, and the response value of the composite material to 2000 ppm CO was raised 13 times than that of pure SnO_2. Turgut et al. [43] synthesized Mo/F double doped SnO_2 films and obtained the best electrical and optical properties. In relation to SnO_2 nanostructures, doping with element Zn has been paid more attention by several groups [14, 44–46]. As previous reports [2, 44], Sn(IV) would form $Sn(OH)_6^{2-}$ ions in highly alkaline solution and then undergo decomposition to obtain SnO_2 nuclei. After introduction of Zn^{2+} into the reaction mixture, different morphologies of Zn-doped SnO_2 nanostructures can be formed. Jia et al. [44] synthesized Zn-doped SnO_2 hierarchical architectures assembled by nanocones via a solvothermal approach. Li et al. [47] reported that Zn-doped SnO_2 nanostructures are composed of dense SnO_2 nanowires with growth orientation along the (101) direction. Huang et al. [14] modified the morphologies and properties of the flower-like single-crystalline SnO_2 nanorods by Zn doping in a facile hydrothermal synthesis route without any complex or toxic organic reagents. After Zn doping, the morphology changed from nanorods with a constant diameter (Figures 6(a) and 6(b)) to needle-like nanorods (Figures 6(c) and 6(d)). The needle-like nanorods are of smooth surfaces and rectangular cross section with a diameter of 30–50 nm and a length up to several hundred nanometers. The lattice spacing of crystallographic planes marked in the image (Figure 6(f)) has been measured to be 0.35 nm and 0.27 nm, respectively, corresponding to the (110) and (101) planes of rutile SnO_2. In addition, doping of other elements, such as Co and Fe, was also synthesized by a chemical route using polyvinyl alcohol as surfactant [23]. Moreover, Wang et al. [48] have reported the synthesis of hierarchical SnO_2 nanoflowers using NaF as the morphology-controlling agent and $SnCl_2{\cdot}2H_2O$ as the tin source. This resulted in the simultaneous Sn^{2+} self-doping of SnO_2 nanostructures and led to the formation of tunable

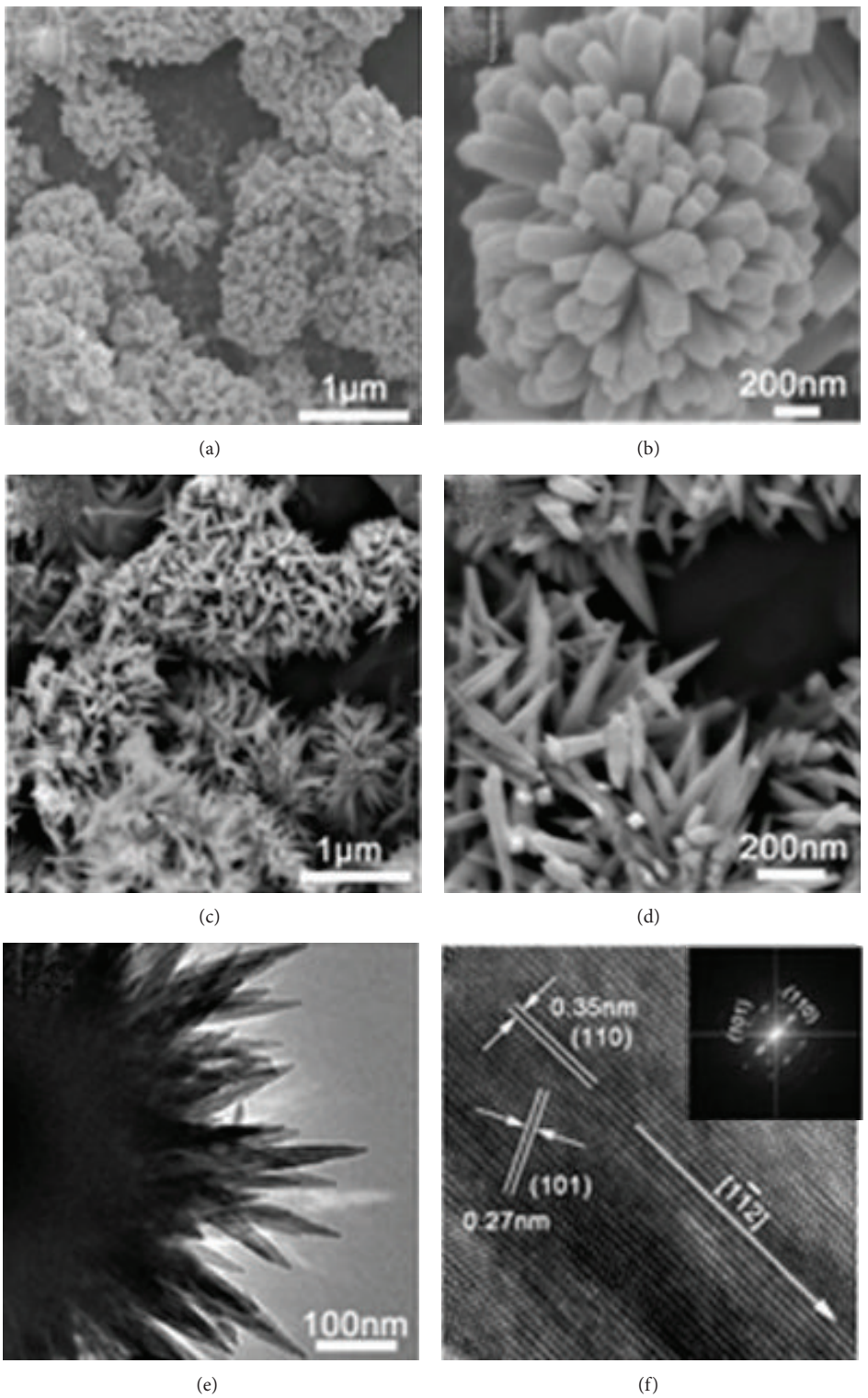

Figure 6: SEM and TEM images of pure SnO_2 nanorods and Zn-doped SnO_2 nanorods. ((a), (b)) SEM image of pure SnO_2 nanorods, ((c), (d)) SEM image of Zn-doped SnO_2 nanorods, (e) TEM image, and (f) HRTEM image of a typical nanorod. Inset in (f) is the fast Fourier transform (FFT) of the HRTEM image adapted from [14] with permission.

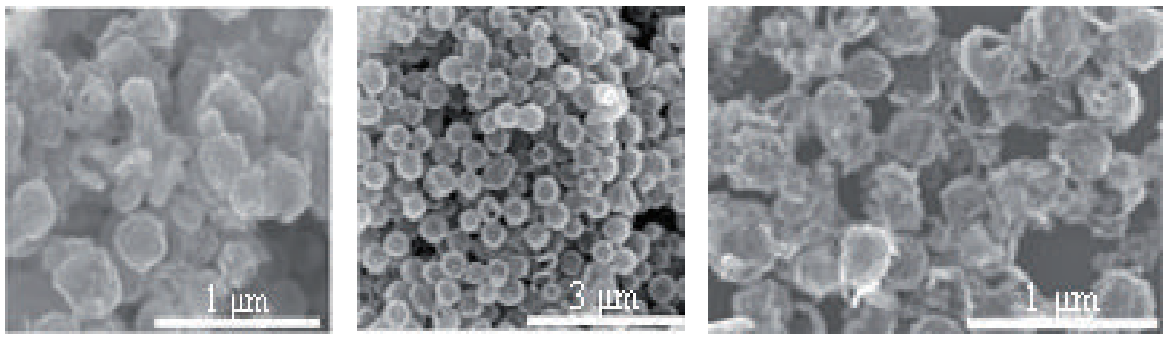

(a) (b) (c)

Figure 7: SEM images of WO_3-SnO_2 HNS nanocomposites with different added amounts of Na_2SnO_3. (a) 0.2 mmol, (b) 0.5 mmol, and (c) 1 mmol adapted from [52] with permission.

oxygen vacancies bandgap states and the corresponding shifting in the semiconductor Fermi levels and further extended absorption in the visible spectral range.

2.3. SnO_2-Based Nanocomposites. Recently, many researchers have reported the fabrication of sensitized semiconductor by noble metal particles or the formation of semiconductor heterojunction, in which the performance can be greatly improved. Chung et al. [49] synthesized Au@ZnO core-shell structure for gaseous formaldehyde sensing at room temperature. The sensor response of the Au@ZnO core-shell structure was enhanced to 10.57 from 1.91 of the pure ZnO. Ju et al. [28] prepared NiO/ZnO PN heterojunction TEA gas sensor and the response is much higher than that of pure ZnO nanosheet sensor and other reported oxide chemiresistive gas sensors. Herein, SnO_2-based nanocomposites have been actively pursued in order to improve their performance in gas sensors [50, 51], dye-sensitized solar cells [47], and so on. Li et al. [51] prepared the composites of SnO_2 nanocrystal/graphene-nanosheets on the basis of the reduction of graphene oxide (GO) by Sn^{2+} ion. The morphologies of SnO_2/graphene-nanosheets composites were changed with different ratios of Sn^{2+} and GO. Li et al. [52] synthesized WO_3-SnO_2 hollow nanospheres by hydrothermal process with a diameter and thickness of about 550 nm and 30 nm, respectively. The influence of the Na_2SnO_3 concentrations on the morphologies of nanocomposites was investigated due to its alkaline nature Na_2SnO_3 which may control the hydrolysis degree of Na_2WO_4, as shown in Figure 7. When the reaction was carried out with 0.2 mmol Na_2SnO_3, a small number of nanospheres coexisted with irregular aggregates of nanoparticles (Figure 7(a)). As the amount of Na_2SnO_3 was increased to 0.5 mmol, the obtained product consisted of large nanospheres (Figure 7(b)). However, particles aggregated without an orderly shape were collected when the amount of Na_2SnO_3 increased to 1 mmol, as shown in Figure 7(c).

Besides, the composites of SnO_2 nanostructures with other materials such as Fe_2O_3, CuO, and ZnO have also been reported. Liu et al. [53] demonstrated the growth of Fe_2O_3@SnO_2 nanoparticle decorated graphene flexible films. Choi et al. [54] prepared CuO-loaded SnO_2 hollow spheres by ultrasonic spray pyrolysis. Moreover, ZnO-SnO_2 nanocomposites have been also investigated in some reports [55, 56].

2.4. Stannate Nanomaterials. Stannate nanomaterials like $ZnSnO_3$ [57, 58], Zn_2SnO_4 [59, 60], and $CdSnO_3$ [61] have also attracted much more attention for higher reversible capacities, low cost, easy preparation, and especially various morphologies [58–61]. Wang et al. [61] synthesized highly porous $CdSnO_3$ nanoparticles using citric acid (Figure 8) and applied it as an anode material for rechargeable LIBs. It can be seen that there was a sharp contrast between the bright cavities and dark edges, which further confirmed the formation of the porous structure (Figures 8(a), 8(b), and 8(c)). For the $CdSnO_3$ nanoparticles, the HRTEM images showed lattice fringes spacing of *ca.* 0.1996 nm, corresponding to the (024) planes of rhombohedral-phase $CdSnO_3$ (Figure 8(d)).

Zn_2SnO_4 have also drawn much attention as anode materials [27]. Zhao et al. [62] fabricated monodispersed hollow Zn_2SnO_4 boxes by the simple coprecipitation and alkali etching way. The hollow boxes exhibit an electrochemical performance with high capacity and good cycling stability than the solid cubes and those reported. Wang et al. [60] prepared flower-like Zn_2SnO_4 composites through a green hydrothermal synthesis, in which the flower-like Zn_2SnO_4 structures are composed of several 1D Zn_2SnO_4 nanorods. These structures generally consist of several sharp tips branching out in three dimensions with large surface area. Duan et al. [58] fabricated amorphous $ZnSnO_3$ hollow nanoboxes for the first time in a large scale by a facile alkaline solution etching method.

3. Applications of SnO_2-Based Nanomaterials

3.1. Lithium-Ion Batteries. In order to address both energy and power demands, there is an urgent need to develop clean energy sources systems. Herein, LIBs have attracted widespread attention because of their high energy density, high power, smooth discharge, and light weight as well as being environment friendly [63]. The electrode's material is one of the key components for perfecting LIBs. It plays a crucial role in establishing the overall properties of the

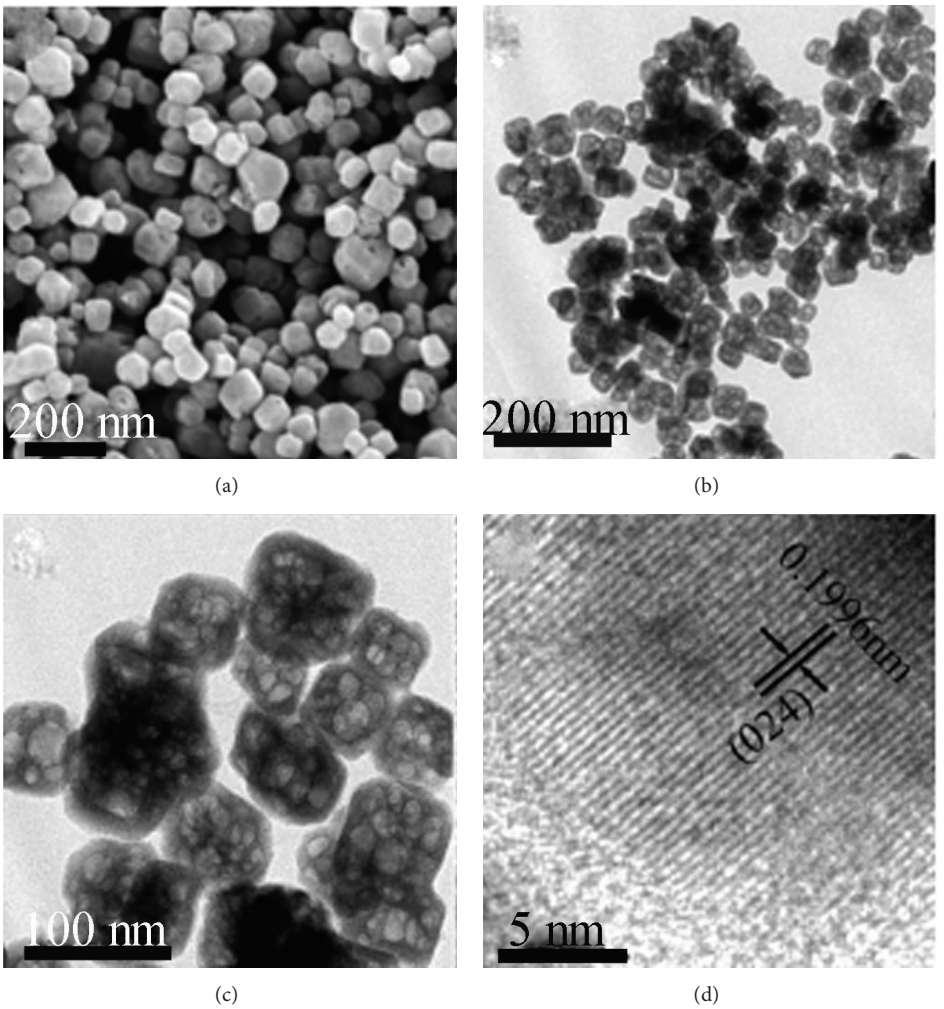

Figure 8: SEM and TEM images of $CdSnO_3$: (a) an SEM image, (b) low-magnification and (c) high-magnification TEM images, and (d) HRTEM image, adapted from [61] with permission.

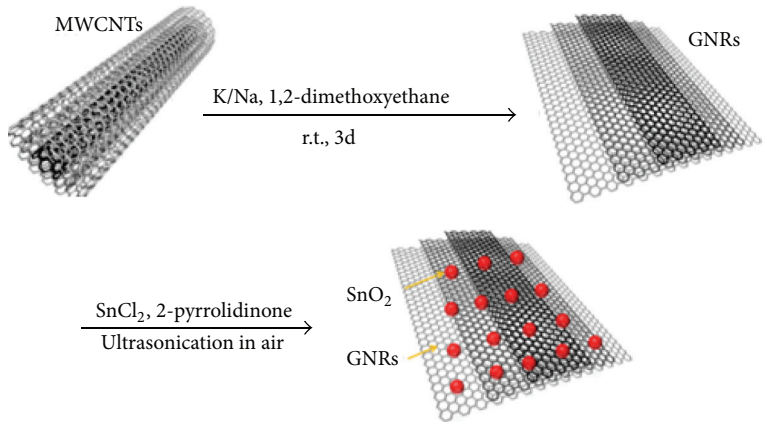

Figure 9: Scheme for the synthesis of the GNRs/SnO_2 composite, adapted from [78] with permission.

battery. SnO_2 has been demonstrated to be one of the most promising anode materials for high performance LIBs [33, 64–66], due to its high theoretical specific storage capacity (782 mAh/g), compared with the commercially used graphite (372 mAh/g) [67, 68]. The mechanism of LIBs for SnO_2 is based on the alloying/dealloying processes, which are the

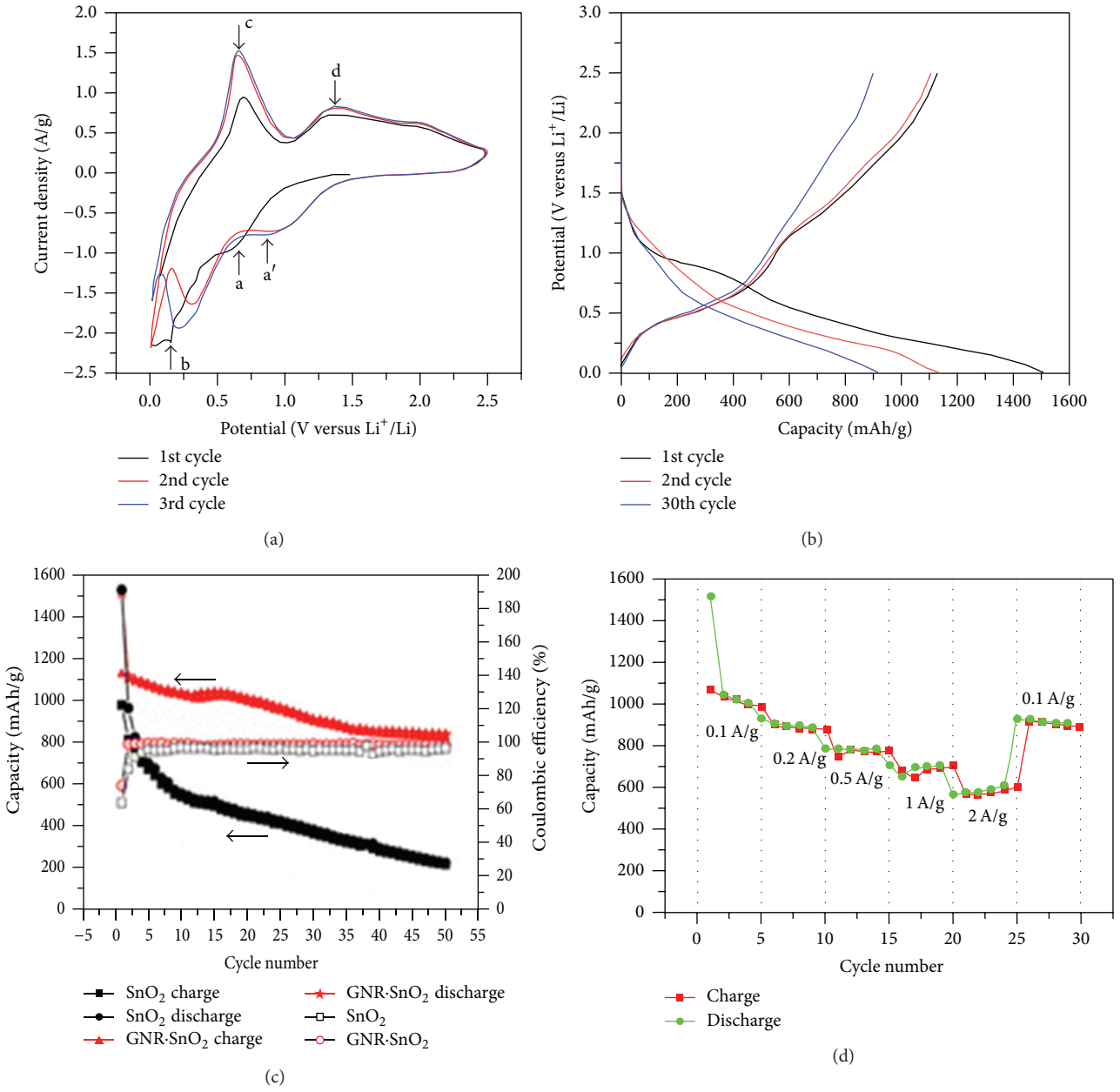

FIGURE 10: The electrochemical performance of the GNRs/SnO_2 composite electrodes. The specific capacities are calculated based on the total mass of the GNRs/SnO_2 composite in the anode electrodes: (a) CV curves of the first, second, and third cycles of the composite electrodes at a scan rate of 0.5 mV/s over the voltage range of 0.01~2.5 V. (b) The first, second, and 30th charge/discharge curves of the composite electrode at a rate of 100 mA/g. (c) Comparison of capacity retention and Coulombic efficiency of GNRs and the GNRs/SnO_2 composite at a rate of 100 mA/g. (d) Rate capability of the composite electrodes with various current densities adapted from [78] with permission.

intrinsic driving force for the electrochemical activity [68, 69]:

$$SnO_2 + 4Li^+ + 4e^{-1} \longrightarrow Sn + 2Li_2O \quad (6)$$

$$Sn + \chi Li^+ + \chi e^{-1} \longleftrightarrow Li_\chi Sn \quad (0 \le \chi \le 4.4) \quad (7)$$

However, the lithiation/delithiation process often induces the large volume expansion and further causes pulverization. This will lead to severe internal strain, cracking, and blocking of the electrical contact pathways in the electrodes, which result in their rapid deterioration and low retention of the electrical capacity [70, 71]. To overcome the above problems, many efforts have been carried out to optimize the structures, compositions, and morphologies of SnO_2-based materials, such as 0D nanoparticles [64, 72], 1D nanowires [73], 2D nanosheets [35], and the doping [74, 75] or composition [76] with other materials.

Wu et al. [22] reported that hierarchical SnO_2 nanostructures that consist of SnO_2 nanosheets exhibit superior reversible capacities (discharge capacity of 516 mAh/g) and

cyclic capacity retention (80%) after 50 cycles at a current rate of 400 mA/g, which is much higher than that of commercial SnO_2 nanoparticles (286 mA/g, 48% retention). This can be ascribed to its stable porous structure. The high porosity, short transport paths of SnO_2 nanosheets, and the interconnections between the individual building blocks of such hierarchical structures endow those promising candidates as anode materials for LIBs. Wang et al. [77] fabricated N-doped G-SnO_2 sandwich papers. The sandwich structure not only assures solid contact between the SnO_2 particle and the graphene layer, but also facilitates high electrode conductivity and renders the elastomeric space needed to accommodate the volume changes of SnO_2. When this material is used in LIBs, it exhibits a very large capacity, high rate capability, and excellent cycling stability. All the excellent electrochemical performances of this material with respect to commercial SnO_2 nanoparticles can be attributed to the structural features that provide a large number of surface defects induced onto the graphene by N-doping, excellent electronic conductivity, short transportation length for both lithium ions and electrons, and enough elastomeric space to accommodate volume changes upon Li insertion/extraction. Lin et al. [78] synthesized a composite made from graphene nanoribbons (GNRs) and SnO_2 nanoparticles used as the anode material for LIBs. The synthesis route of the GNRs/SnO_2 composite is illustrated in Figure 9. First, the GNRs were obtained using K/Na alloy to unzip the MWCNTs. Then, $SnCl_2$ and 2-pyrrolidinone were added into the GNRs with ultrasonication for reducing Sn^{2+} to Sn^0. Lastly, the Sn NPs were oxidized overnight using ultrasonication in air. The CV curves of the initial three cycles show the reversibility of the composite electrode charge/discharge process, as shown in Figure 10(a). The composite, as an anode material for LIBs, exhibits reversible capacities of over 1520 and 1130 mAh/g for the first discharge and charge, respectively, which is more than the theoretical capacity of SnO_2 (Figure 10(b)). The reversible capacity retains ~ 825 mAh/g at a current density of 100 mA/g with a Coulombic efficiency of 98% after 50 cycles (Figure 10(c)). Furthermore, the composite shows good power performance with a reversible capacity of ~580 mAh/g at the current density of 2 A/g, as shown in Figure 10(d). The high capacity and good power performance and retention can be attributed to uniformly distributed SnO_2 NPs along the high-aspect-ratio GNRs. The GNRs act as conductive additives that buffer the volume changes of SnO_2 during cycling. This work provides a starting point for exploring the composites made from GNRs and other transition metal oxides for lithium storage applications.

Besides, Yang et al. [79] synthesized SnO_2/graphene nanosheet nanocomposite as an anode material for LIBs. The SnO_2-In_2O_3/GNS nanocomposite exhibits obvious enhancement electrochemical performance in terms of lithium storage capacity (962 mAh/g at 60 mA/g rate), initial Coulombic efficiency (57.2%), cycling stability (60.8% capacity retention after 50 cycles), and rate capability (393.25 mAh/g at 600 mA/g rate after 25 cycles) compared to SnO_2/GNS and pure SnO_2-In_2O_3 electrode.

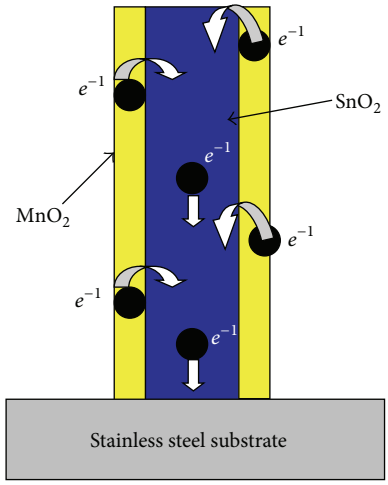

Figure 11: Schematic image of the amorphous MnO_2 loaded on the SnO_2 nanowires grown on the stainless steel substrate. The SnO_2 nanowire provides a direct path for the electrons adapted from [90] with permission.

3.2. Supercapacitors. Supercapacitors, also called electrochemical capacitors, have been known for over than fifty years and considered as one of the most promising energy storage devices for a wide range of uninterruptible power supplies and civilian and military applications in electric vehicles [80–82]. In contrast to conventional capacitors and LIBs, supercapacitors possess much higher energy density and also exhibit higher specific power. Up to now, there are mainly three kinds of electrode materials for supercapacitors which are as follow: metal oxides, carbon, and conducting polymers [83–86]. Due to low cost and environmental compatibility consideration, metal oxide candidates with good capacitive values have attracted much attention [87].

SnO_2-based supercapacitors have been paid significant attention due to their high electrochemical capacitor (EC) and chemical stability [88, 89]. Yan et al. [90] synthesized SnO_2/MnO_2 composite for the application of supercapacitor electrodes. The prepared process was shown in Figure 11. This nanostructure has several advantages: (1) a thin layer of MnO_2 would enable a fast, reversible faradic reaction and would provide a short ion diffusion path; (2) SnO_2 nanowires, with high conductivity, would provide a direct path for the electrons transport; and (3) SnO_2 nanowires would create channels for the effective transport of electrolyte. Based on the above, it exhibited a specific capacitance (based on MnO_2) as high as 637 F g^{-1} at a scan rate of 2 mV s^{-1} (800 F g^{-1} at a current density of 1 A g^{-1}) in 1 M Na_2SO_4 aqueous solution (Figure 12(a)). Temperature is an important influence factor on supercapacitor cells. It is valuable to evaluate the capacitive behavior of SnO_2/MnO_2 composites at various temperatures. Figure 12(b) shows the specific capacitance obtained at different temperatures and scan rates. It can be seen obviously that the specific capacitance and rate capability increase with the increase of temperature. This is attributed to the decrease of effective internal resistance with increasing temperature. The energy density

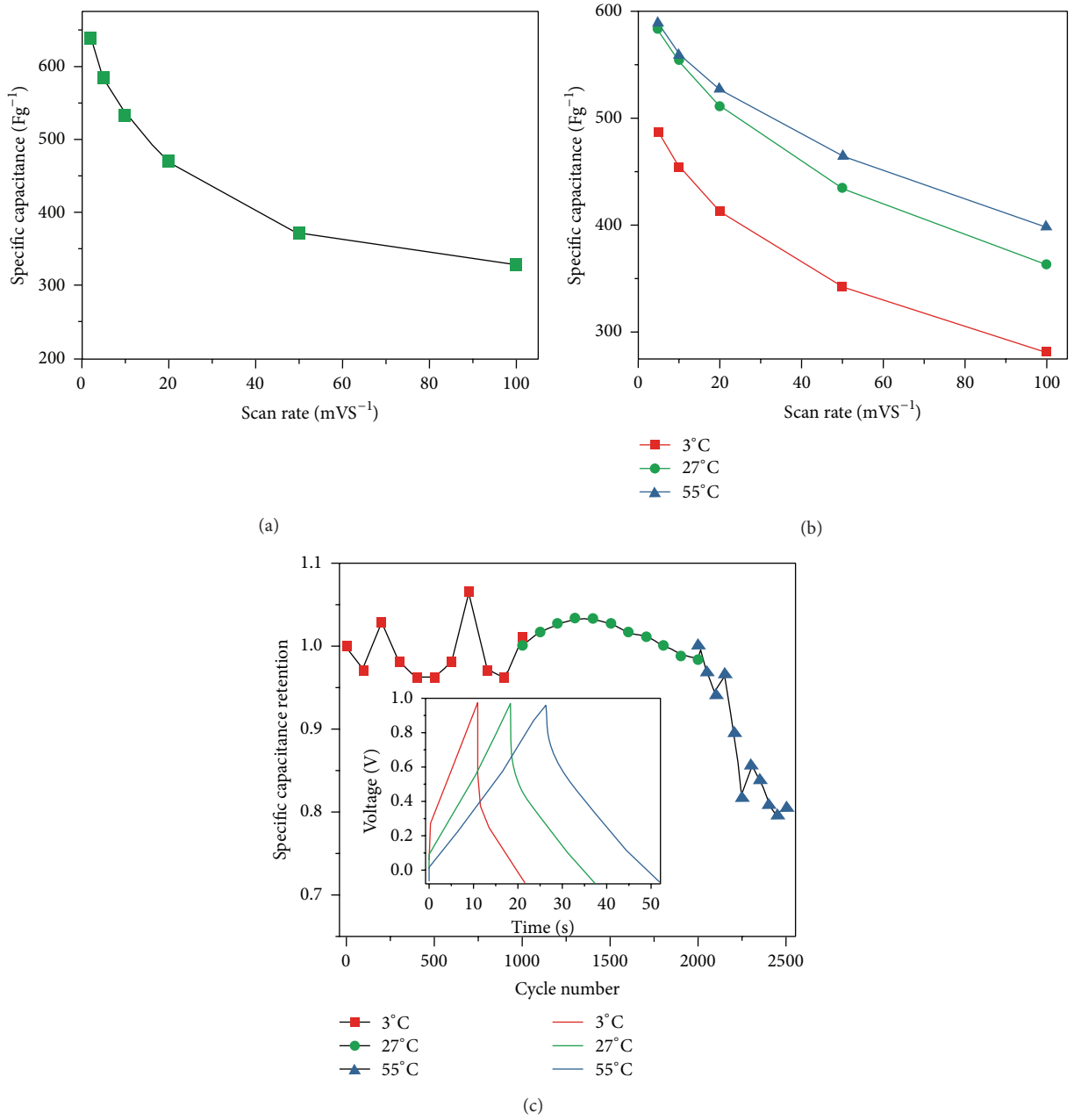

FIGURE 12: (a) Plotted curve of the variation in the specific capacitance of the SnO_2/MnO_2 composites as a function of the scan rate. (b) Specific capacitance obtained at different scan rates at 3, 27, and 55°C. (c) Curve showing long-term stability as a function of the cycle number tested by constant current charge/discharge method (current density of 20 A g^{-1}), which was carried out continuously at 3 ± 1°C (ice water bath) and then at 27°C (room temperature) and finally at 55 ± 2°C (water bath). The inset shows the first cycle of charge/discharge curves at different temperatures at a high current density of 20 A g^{-1} adapted from [90] with permission.

and power density measured at 50 A g^{-1} are 35.4 W h kg^{-1} and 25 kW kg^{-1}, respectively, demonstrating a good rate capability. After that, the SnO_2/MnO_2 composite electrode shows an excellent long-term cyclic stability (less than 1.2% decrease of the specific capacitance is observed after 2000 CV cycles), as shown in Figure 12(c). Li et al. [89] fabricated Fe_3O_4@SnO_2 core-shell nanorods. The hybrid nanorod film displayed well-defined electrochemical features in Na_2SO_4 aqueous electrolyte, charging/discharging within seconds and with much higher areal capacitance (7.013 mF cm^{-2} at 0.20 mA cm^{-2}) than pristine Fe_3O_4 nanorod film. In addition, the PANI/SnO_2 composite electrode exhibited specific capacitance of 173 F g^{-1} at a scan rate of 25 mV s^{-1} [8, 91]. Bao et al. [92] designed Zn_2SnO_4/MnO_2 core/shell nanocable-carbon microfiber hybrid composites for high-performance supercapacitor electrodes. The hybrid composite exhibited excellent rate capability with specific energy of 36.8 Wh/kg and specific power of 32 kW/kg at current density of 40 A/g,

respectively, as well as good long-term cycling stability (only 1.2% loss of its initial specific capacitance after 1000 cycles).

Moreover, compared with other materials, graphene has been used as the electrode of electrochemical supercapacitors (ESCs), due to its good capacitive performance, superior conductivity, large surface-to-volume ratio, and suitable pore size distribution [93]. As we know, carbon and metal oxide materials are two hotspots as electrode materials for electrochemical supercapacitors (ESCs), in which energy can be stored due to the formation of an electrical double layer at the interface of the electrode. If integrating the above two kinds of materials into the electrodes of ESCs, their capacitive performance will be greatly enhanced because most of the metal oxide can contribute pseudo-capacitance to the total capacitance apart from the double-layer capacitance from carbon materials [94–96]. Thus, combined SnO_2 with graphene for the supercapacitors can obviously enhance the performance of capacitance. Li et al. [51] synthesized SnO_2/graphene (SnO_2/G) nanocomposites by a facile solvent-based synthesis route based on the oxidation-reduction reaction. The electrochemical performance of SnO_2/graphene showed an excellent specific capacitance of 363.3 F g^{-1}, which was five-fold higher than that of the as-synthesized graphene (68.4 F g^{-1}). El-Deen et al. [97] fabricated graphene/SnO_2 nanocomposite which exhibited high specific capacitance (323 F g^{-1}), excellent cycling stability, very good salt removal efficiency (83%), and distinct electrosorptive capacity of 1.49 mg g^{-1}.

4. Conclusion

In this paper, we discussed the synthesis of phase-pure SnO_2 hierarchical structures with different morphologies including nanoparticles, nanorods, nanosheets, nanosphere, and the porous and hollow structures. We also reviewed their modifications by doping and compositing with other materials and synthesis of stannate nanomaterials. Reaction parameters such as the chemical state of the tin precursors (Sn(IV) versus Sn(II) salts), concentration, additives, and solvents play an important role in adjusting their morphologies. SnO_2-based nanostructures, such as anode materials, demonstrate superior cycle performance of lithium storage by doping. In the supercapacitors, the prepared SnO_2-based nanostructures provide fast ion and electron transfer, which led to a prominent supercapacitor performance. Therefore, SnO_2-based nanostructures with a proper design can possess advanced physical and chemical properties, which are vital for a variety of energy and environment applications.

Although significant progress has been made in the synthesis of SnO_2-based nanostructures, further efforts are still required to understand the mechanism of doping and nanocomposites better, which are still unclear but crucial for the design of SnO_2-based nanostructures in enhancement of their lithium storage, supercapacitors, and energy conversion performance. After the introduction of components with different chemical compositions, SnO_2-based nanomaterials got wide applications. However, it is still a challenge in the large-scale synthesis of SnO_2 nanocrystals with more specific facets exposed. We hope that the present paper will further expand the applications of SnO_2-based nanostructures to meet the environment- and energy-related demands.

Conflict of Interests

The authors declare that there is no conflict of interests regarding the publication of this paper.

Acknowledgments

The authors thank the University of Jinan (UJN) for the support on new staff, and the project was supported by the Taishan Scholar (no. TSHW20120210), the National Natural Science Foundation of China (Grant no. 11304120), and the Encouragement Foundation for Excellent Middle-aged and Young Scientist of Shandong Province (Grant no. BS2012CL005).

References

[1] J. S. Chen and X. W. Lou, "SnO_2-based nanomaterials: synthesis and application in lithium-ion batteries," *Small*, vol. 9, no. 11, pp. 1877–1893, 2013.

[2] Y. Liu, Y. Jiao, Z. Zhang, F. Qu, A. Umar, and X. Wu, "Hierarchical SnO_2 nanostructures made of intermingled ultrathin nanosheets for environmental remediation, smart gas sensor, and supercapacitor applications," *ACS Applied Materials and Interfaces*, vol. 6, no. 3, pp. 2174–2184, 2014.

[3] X. W. Lou, C. M. Li, and L. A. Archer, "Designed synthesis of coaxial SnO_2@carbon hollow nanospheres for highly reversible lithium storage," *Advanced Materials*, vol. 21, no. 24, pp. 2536–2539, 2009.

[4] S.-L. Chou, J.-Z. Wang, H.-K. Liu, and S.-X. Dou, "SnO_2 meso-scale tubes: one-step, room temperature electrodeposition synthesis and kinetic investigation for lithium storage," *Electrochemistry Communications*, vol. 11, no. 2, pp. 242–246, 2009.

[5] Y. Han, X. Wu, Y. Ma, L. Gong, F. Qu, and H. Fan, "Porous SnO_2 nanowire bundles for photocatalyst and Li ion battery applications," *CrystEngComm*, vol. 13, no. 10, pp. 3506–3510, 2011.

[6] P. Meduri, C. Pendyala, V. Kumar, G. U. Sumanasekera, and M. K. Sunkara, "Hybrid tin oxide nanowires as stable and high capacity anodes for li-ion batteries," *Nano Letters*, vol. 9, no. 2, pp. 612–616, 2009.

[7] S. N. Pusawale, P. R. Deshmukh, and C. D. Lokhande, "Chemical synthesis of nanocrystalline SnO_2 thin films for supercapacitor application," *Applied Surface Science*, vol. 257, no. 22, pp. 9498–9502, 2011.

[8] Y. L. Gao, J. X. Wu, W. Zhang et al., "SO_4^{2+}/SnO_2 as a new electrode for electrochemical supercapacitors," *Ceramics International*, vol. 40, no. 6, pp. 8925–8929, 2014.

[9] X. Meng, M. Zhou, X. Li et al., "Synthesis of SnO_2 nanoflowers and electrochemical properties of Ni/SnO_2 nanoflowers in supercapacitor," *Electrochimica Acta*, vol. 109, no. 30, pp. 20–26, 2013.

[10] S. Faraji and F. N. Ani, "Microwave-assisted synthesis of metal oxide/hydroxide composite electrodes for high power supercapacitors—a review," *Journal of Power Sources*, vol. 263, pp. 338–360, 2014.

[11] J. Zhang, J. Guo, H. Xu, and B. Cao, "Reactive-template fabrication of porous SnO_2 nanotubes and their remarkable gas-sensing performance," *ACS Applied Materials & Interfaces*, vol. 5, no. 16, pp. 7893–7898, 2013.

[12] Y. Jia, L. He, Z. Guo et al., "Preparation of porous tin oxide nanotubes using carbon nanotubes as templates and their gas-sensing properties," *Journal of Physical Chemistry C*, vol. 113, no. 22, pp. 9581–9587, 2009.

[13] X. Wang, H. Fan, and P. Ren, "Self-assemble flower-like SnO_2/Ag heterostructures: correlation among composition, structure and photocatalytic activity," *Colloids and Surfaces A: Physicochemical and Engineering Aspects*, vol. 419, no. 20, pp. 140–146, 2013.

[14] H. Huang, S. Tian, J. Xu et al., "Needle-like Zn-doped SnO_2 nanorods with enhanced photocatalytic and gas sensing properties," *Nanotechnology*, vol. 23, no. 10, Article ID 105502, 2012.

[15] S. Chen, M. Wang, J. Ye et al., "Kinetics-controlled growth of aligned mesocrystalline SnO_2 nanorod arrays for lithium-ion batteries with superior rate performance," *Nano Research*, vol. 6, no. 4, pp. 243–252, 2013.

[16] B. Cheng, J. M. Russell, W. Shi, L. Zhang, and E. T. Samulski, "Large-Scale, Solution-Phase Growth of Single-Crystalline SnO_2 Nanorods," *Journal of the American Chemical Society*, vol. 126, no. 19, pp. 5972–5973, 2004.

[17] N. Talebian and F. Jafarinezhad, "Morphology-controlled synthesis of SnO_2 nanostructures using hydrothermal method and their photocatalytic applications," *Ceramics International*, vol. 39, no. 7, pp. 8311–8317, 2013.

[18] Z. R. Dai, J. L. Gole, J. D. Stout, and Z. L. Wang, "Tin oxide nanowires, nanoribbons, and nanotubes," *Journal of Physical Chemistry B*, vol. 106, no. 6, pp. 1274–1279, 2002.

[19] X. L. Wang, N. Aroonyadet, Y. Z. Zhang et al., "Aligned epitaxial SnO_2 nanowires on sapphire: growth and device applications," *Nano Letters*, vol. 14, no. 6, pp. 3014–3022, 2014.

[20] Z. Yang, G. Du, Q. Meng et al., "Dispersion of SnO_2 nanocrystals on TiO_2(B) nanowires as anode material for lithium ion battery applications," *RSC Advances*, vol. 1, no. 9, pp. 1834–1840, 2011.

[21] X. Li, X. Meng, J. Liu et al., "Tin oxide with controlled morphology and crystallinity by atomic layer deposition onto graphene nanosheets for enhanced lithium storage," *Advanced Functional Materials*, vol. 22, no. 8, pp. 1647–1654, 2012.

[22] H. B. Wu, J. S. Chen, X. W. Lou, and H. H. Hng, "Synthesis of SnO_2 hierarchical structures assembled from nanosheets and their lithium storage properties," *Journal of Physical Chemistry C*, vol. 115, no. 50, pp. 24605–24610, 2011.

[23] Y. Gao and Z. Tang, "Design and application of inorganic nanoparticle superstructures: current status and future challenges," *Small*, vol. 7, no. 15, pp. 2133–2146, 2011.

[24] W. Shi, S. Song, and H. Zhang, "Hydrothermal synthetic strategies of inorganic semiconducting nanostructures," *Chemical Society Reviews*, vol. 42, no. 13, pp. 5714–5743, 2013.

[25] J. Kaur, J. Shah, R. K. Kotnala, and K. C. Verma, "Raman spectra, photoluminescence and ferromagnetism of pure, Co and Fe doped SnO_2 nanoparticles," *Ceramics International*, vol. 38, no. 7, pp. 5563–5570, 2012.

[26] J. M. D. Coey, A. P. Douvalis, C. B. Fitzgerald, and M. Venkatesan, "Ferromagnetism in Fe-doped SnO_2 thin films," *Applied Physics Letters*, vol. 84, no. 8, pp. 1332–1334, 2004.

[27] Y. Zhao, Y. Huang, Q. Wang et al., "Hollow Zn_2SnO_4 boxes coated with N-doped carbon for advanced lithium-ion batteries," *Ceramics International*, vol. 40, no. 1, pp. 2275–2280, 2014.

[28] D. Ju, H. Xu, Z. Qiu, J. Guo, J. Zhang, and B. Cao, "Highly sensitive and selective triethylamine-sensing properties of nanosheets directly grown on ceramic tube by forming NiO/ZnO PN heterojunction," *Sensors and Actuators, B: Chemical*, vol. 200, pp. 288–296, 2014.

[29] F. Du, Z. Guo, and G. Li, "Hydrothermal synthesis of SnO_2 hollow microspheres," *Materials Letters*, vol. 59, no. 19-20, pp. 2563–2565, 2005.

[30] G. Xi and J. Ye, "Ultrathin SnO_2 nanorods: template- and surfactant-free solution phase synthesis, growth mechanism, optical, gas-sensing, and surface adsorption properties," *Inorganic Chemistry*, vol. 49, no. 5, pp. 2302–2309, 2010.

[31] J. Ye, H. Zhang, R. Yang, X. Li, and L. Qi, "Morphology-controlled synthesis of SnO_2 nanotubes by using 1D silica mesostructures as sacrificial templates and their applications in lithium-ion batteries," *Small*, vol. 6, no. 2, pp. 296–306, 2010.

[32] B. Liu and H. C. Zeng, "Salt-assisted deposition of SnO_2 on α-moO_3 nanorods and fabrication of polycrystalline SnO_2 nanotubes," *Journal of Physical Chemistry B*, vol. 108, no. 19, pp. 5867–5874, 2004.

[33] Y. Wang, H. C. Zeng, and J. Y. Lee, "Highly reversible lithium storage in porous SnO_2 nanotubes with coaxially grown carbon nanotube overlayers," *Advanced Materials*, vol. 18, no. 5, pp. 645–649, 2006.

[34] N. Du, H. Zhang, J. Chen, J. Sun, B. Chen, and D. Yang, "Metal oxide and sulfide hollow spheres: layer-by-layer synthesis and their application in lithium-ion battery," *Journal of Physical Chemistry B*, vol. 112, no. 47, pp. 14836–14842, 2008.

[35] X. M. Yin, C. C. Li, M. Zhang et al., "One-step synthesis of hierarchical SnO_2 hollow nanostructures via self-assembly for high power lithium ion batteries," *Journal of Physical Chemistry C*, vol. 114, no. 17, pp. 8084–8088, 2010.

[36] H. Wang, J. Liang, H. Fan et al., "Synthesis and gas sensitivities of SnO_2 nanorods and hollow microspheres," *Journal of Solid State Chemistry*, vol. 181, no. 1, pp. 122–129, 2008.

[37] D. S. Jung, Y. N. Ko, Y. C. Kang, and S. B. Park, "Recent progress in electrode materials produced by spray pyrolysis for next-generation lithium ion batteries," *Advanced Powder Technology*, vol. 25, no. 1, pp. 18–31, 2014.

[38] Y. J. Hong, J.-W. Yoon, J.-H. Lee, and Y. C. Kang, "One-pot synthesis of Pd-loaded SnO_2 yolk-shell nanostructures for ultraselective methyl benzene sensors," *Chemistry*, vol. 20, no. 10, pp. 2737–2741, 2014.

[39] L. A. Patil, M. D. Shinde, A. R. Bari, and V. V. Deo, "Novel trapping system for size wise sorting of SnO_2 nanoparticles synthesized from pyrolysis of ultrasonically atomized spray for gas sensing," *Sensors and Actuators, B: Chemical*, vol. 143, no. 1, pp. 316–324, 2009.

[40] S. H. Ju, H. C. Jang, and Y. C. Kang, "Characteristics of nano-sized tin dioxide powders prepared by spray pyrolysis," *Journal of the Ceramic Society of Japan*, vol. 117, no. 1368, pp. 922–925, 2009.

[41] W. Yan, M. Fang, X. Tan et al., "Template-free fabrication of SnO_2 hollow spheres with photoluminescence from Sni," *Materials Letters*, vol. 64, no. 19, pp. 2033–2035, 2010.

[42] X.-T. Yin and X.-M. Guo, "Selectivity and sensitivity of Pd-loaded and Fe-doped SnO_2 sensor for CO detection," *Sensors and Actuators, B: Chemical*, vol. 200, pp. 213–218, 2014.

[43] G. Turgut, E. Sonmez, S. Aydin, R. Dilber, and U. Turgut, "The effect of Mo and F double doping on structural, morphological, electrical and optical properties of spray deposited SnO_2 thin

films," *Ceramics International*, vol. 40, no. 8, pp. 12891–12898, 2014.

[44] T. Jia, W. Wang, F. Long, Z. Fu, H. Wang, and Q. Zhang, "Synthesis, characterization, and photocatalytic activity of Zn-doped SnO_2 hierarchical architectures assembled by nanocones," *Journal of Physical Chemistry C*, vol. 113, no. 21, pp. 9071–9077, 2009.

[45] M. Torabi and S. K. Sadrnezhaad, "Electrochemical evaluation of nanocrystalline Zn-doped tin oxides as anodes for lithium ion microbatteries," *Journal of Power Sources*, vol. 196, no. 1, pp. 399–404, 2011.

[46] X. Liu, J. Iqbal, Z. Wu, B. He, and R. Yu, "Structure and room-temperature ferromagnetism of Zn-doped SnO_2 nanorods prepared by solvothermal method," *The Journal of Physical Chemistry C*, vol. 114, no. 11, pp. 4790–4796, 2010.

[47] Z. Li, Y. Zhou, T. Yu, J. Liu, and Z. Zou, "Unique Zn-doped SnO_2 nano-echinus with excellent electron transport and light harvesting properties as photoanode materials for high performance dye-sensitized solar cell," *CrystEngComm*, vol. 14, no. 20, pp. 6462–6468, 2012.

[48] H. Wang, K. Dou, W. Y. Teoh et al., "Engineering of facets, band structure, and gas-sensing properties of hierarchical Sn^{2+}-Doped SnO_2 nanostructures," *Advanced Functional Materials*, vol. 23, no. 38, pp. 4847–4853, 2013.

[49] F.-C. Chung, Z. Zhu, P.-Y. Luo, R.-J. Wu, and W. Li, "Au@ZnO core-shell structure for gaseous formaldehyde sensing at room temperature," *Sensors and Actuators B: Chemical*, vol. 199, pp. 314–319, 2014.

[50] B. Mondal, B. Basumatari, J. Das, C. Roychaudhury, H. Saha, and N. Mukherjee, "ZnO-SnO_2 based composite type gas sensor for selective hydrogen sensing," *Sensors and Actuators B: Chemical*, vol. 194, pp. 389–396, 2014.

[51] Y. Li, X. Lv, J. Lu, and J. Li, "Preparation of SnO_2-nanocrystal/graphene-nanosheets composites and their lithium storage ability," *The Journal of Physical Chemistry C*, vol. 114, no. 49, pp. 21770–21774, 2010.

[52] H. Li, B. Liu, D. Cai et al., "High-temperature humidity sensors based on WO_3-SnO_2 composite hollow nanospheres," *Journal of Materials Chemistry A*, vol. 2, no. 19, pp. 6854–6862, 2014.

[53] S. Liu, R. Wang, M. Liu et al., "Fe_2O_3@SnO_2 nanoparticle decorated graphene flexible films as high-performance anode materials for lithium-ion batteries," *Journal of Materials Chemistry A*, vol. 2, no. 13, pp. 4598–4604, 2014.

[54] K.-I. Choi, H.-J. Kim, Y. C. Kang, and J.-H. Lee, "Ultraselective and ultrasensitive detection of H_2S in highly humid atmosphere using CuO-loaded SnO_2 hollow spheres for real-time diagnosis of halitosis," *Sensors and Actuators B: Chemical*, vol. 194, pp. 371–376, 2014.

[55] A. Hamrouni, H. Lachheb, and A. Houas, "Synthesis, characterization and photocatalytic activity of ZnO-SnO_2 nanocomposites," *Materials Science and Engineering B*, vol. 178, no. 20, pp. 1371–1379, 2013.

[56] W. W. Wang, Y. J. Zhu, and L. X. Yang, "ZnO-SnO_2 hollow spheres and hierarchical nanosheets: hydrothermal preparation, formation mechanism, and photocatalytic properties," *Advanced Functional Materials*, vol. 17, no. 1, pp. 59–64, 2007.

[57] B. Geng, C. Fang, F. Zhan, and N. Yu, "Synthesis of polyhedral $ZnSnO_3$ microcrystals with controlled exposed facets and their selective gas-sensing properties," *Small*, vol. 4, no. 9, pp. 1337–1343, 2008.

[58] J.-F. Duan, S.-C. Hou, S.-G. Chen, and H.-G. Duan, "Synthesis of amorphous $ZnSnO_3$ hollow nanoboxes and their lithium storage properties," *Materials Letters*, vol. 122, pp. 261–264, 2014.

[59] W. Cun, W. Xinming, Z. Jincai et al., "Synthesis, characterization and photocatalytic property of nano-sized Zn_2SnO_4," *Journal of Materials Science*, vol. 37, no. 14, pp. 2989–2996, 2002.

[60] K. Wang, Y. Huang, H. Huang et al., "Hydrothermal synthesis of flower-like Zn_2SnO_4 composites and their performance as anode materials for lithium-ion batteries," *Ceramics International*, vol. 40, no. 6, pp. 8021–8025, 2014.

[61] L. Wang, W. Zhang, C. Wang et al., "A facile synthesis of highly porous $CdSnO_3$ nanoparticles and their enhanced performance in lithium-ion batteries," *Journal of Materials Chemistry A*, vol. 2, no. 14, pp. 4970–4974, 2014.

[62] Y. Zhao, Y. Huang, Q. Wang et al., "Preparation of hollow Zn_2SnO_4 boxes for advanced lithium-ion batteries," *RSC Advances*, vol. 3, no. 34, pp. 14480–14485, 2013.

[63] Y. N. Zhou, M. Z. Xue, and Z. W. Fu, "Nanostructured thin film electrodes for lithium storage and all-solid-state thin-film lithium batteries," *Journal of Power Sources*, vol. 234, pp. 310–332, 2013.

[64] D. Deng and J. Y. Lee, "Hollow core-shell mesospheres of crystalline SnO_2 nanoparticle aggregates for high capacity Li^+ ion storage," *Chemistry of Materials*, vol. 20, no. 5, pp. 1841–1846, 2008.

[65] C. Wang, Y. Zhou, M. Ge, X. Xu, Z. Zhang, and J. Z. Jiang, "Large-scale synthesis of SnO_2 nanosheets with high lithium storage capacity," *Journal of the American Chemical Society*, vol. 132, no. 1, pp. 46–47, 2010.

[66] Z. Wang, D. Luan, F. Y. C. Boey, and X. W. Lou, "Fast formation of SnO_2 nanoboxes with enhanced lithium storage capability," *Journal of the American Chemical Society*, vol. 133, no. 13, pp. 4738–4741, 2011.

[67] X. W. Lou, Y. Wang, C. Yuan, J. Y. Lee, and L. A. Archer, "Template-free synthesis of SnO_2 hollow nanostructures with high lithium storage capacity," *Advanced Materials*, vol. 18, no. 17, pp. 2325–2329, 2006.

[68] H. Wang and A. L. Rogach, "Hierarchical SnO_2 nanostructures: recent advances in design, synthesis, and applications," *Chemistry of Materials*, vol. 26, no. 1, pp. 123–133, 2014.

[69] Y. H. Jin, K. M. Min, S. D. Seo, H. W. Shim, and D. W. Kim, "Enhanced Li storage capacity in 3 nm diameter SnO_2 nanocrystals firmly anchored on multiwalled carbon nanotubes," *Journal of Physical Chemistry C*, vol. 115, no. 44, pp. 22062–22067, 2011.

[70] S. Ding, D. Luan, F. Y. C. Boey, J. S. Chen, and X. W. Lou, "SnO_2 nanosheets grown on graphene sheets with enhanced lithium storage properties," *Chemical Communications*, vol. 47, no. 25, pp. 7155–7157, 2011.

[71] J.-M. Tarascon and M. Armand, "Issues and challenges facing rechargeable lithium batteries," *Nature*, vol. 414, no. 6861, pp. 359–367, 2001.

[72] H.-X. Zhang, C. Feng, Y.-C. Zhai, K.-L. Jiang, Q.-Q. Li, and S.-S. Fan, "Cross-stacked carbon nanotube sheets uniformly loaded with SnO_2 nanoparticles: a novel binder-free and high-capacity anode material for lithium-ion batteries," *Advanced Materials*, vol. 21, no. 22, pp. 2299–2304, 2009.

[73] L.-Y. Jiang, X.-L. Wu, Y.-G. Guo, and L.-J. Wan, "SnO_2-based hierarchical nanomicrostructures: facile synthesis and their applications in gas sensors and lithium-ion batteries," *The Journal of Physical Chemistry C*, vol. 113, no. 32, pp. 14213–14219, 2009.

[74] Y. Wang, I. Djerdj, B. Smarsly, and M. Antonietti, "Antimony-doped SnO_2 nanopowders with high crystallinity for lithium-ion battery electrode," *Chemistry of Materials*, vol. 21, no. 14, pp. 3202–3209, 2009.

[75] X. Wang, X. Cao, L. Bourgeois et al., "N-doped graphene-SnO_2 sandwich paper for high-performance lithium-ion batteries," *Advanced Functional Materials*, vol. 22, no. 13, pp. 2682–2690, 2012.

[76] P. Wu, N. Du, H. Zhang, J. Yu, and D. Yang, "CNTs@SnO_2@C coaxial nanocables with highly reversible lithium storage," *The Journal of Physical Chemistry C*, vol. 114, no. 51, pp. 22535–22538, 2010.

[77] X. Wang, X. Cao, L. Bourgeois et al., "N-doped graphene-SnO_2 sandwich paper for high-performance lithium-ion batteries," *Advanced Functional Materials*, vol. 22, no. 13, pp. 2682–2690, 2012.

[78] J. Lin, Z. Peng, C. Xiang et al., "Graphene nanoribbon and nanostructured SnO_2 composite anodes for lithium ion batteries," *ACS Nano*, vol. 7, no. 7, pp. 6001–6006, 2013.

[79] H. Yang, T. Song, S. Lee et al., "Tin indium oxide/graphene nanosheet nanocomposite as an anode material for lithium ion batteries with enhanced lithium storage capacity and rate capability," *Electrochimica Acta*, vol. 91, pp. 275–281, 2013.

[80] X. Lu, W. Zhang, C. Wang, T.-C. Wen, and Y. Wei, "One-dimensional conducting polymer nanocomposites: synthesis, properties and applications," *Progress in Polymer Science (Oxford)*, vol. 36, no. 5, pp. 671–712, 2011.

[81] S. Sarangapani, B. V. Tilak, and C. P. Chen, "Materials for electrochemical capacitors theoretical and experimental constraints," *Journal of the Electrochemical Society*, vol. 143, no. 11, pp. 3791–3799, 1996.

[82] E. Faggioli, P. Rena, V. Danel, X. Andrieu, R. Mallant, and H. Kahlen, "Supercapacitors for the energy management of electric vehicles," *Journal of Power Sources*, vol. 84, no. 2, pp. 261–269, 1999.

[83] K. W. Nam, W. S. Yoon, and K. B. Kim, "X-ray absorption spectroscopy studies of nickel oxide thin film electrodes for supercapacitors," *Electrochimica Acta*, vol. 47, no. 19, pp. 3201–3209, 2002.

[84] J.-H. Sung, S.-J. Kim, and K.-H. Lee, "Fabrication of microcapacitors using conducting polymer microelectrodes," *Journal of Power Sources*, vol. 124, no. 1, pp. 343–350, 2003.

[85] C. G. Liu, H. T. Fang, F. Li, M. Liu, and H. M. Cheng, "Single-walled carbon nanotubes modified by electrochemical treatment for application in electrochemical capacitors," *Journal of Power Sources*, vol. 160, no. 1, pp. 758–761, 2006.

[86] H. Mi, X. Zhang, X. Ye, and S. Yang, "Preparation and enhanced capacitance of core-shell polypyrrole/polyaniline composite electrode for supercapacitors," *Journal of Power Sources*, vol. 176, no. 1, pp. 403–409, 2008.

[87] C. D. Lokhande, D. P. Dubal, and O. S. Joo, "Metal oxide thin film based supercapacitors," *Current Applied Physics*, vol. 11, no. 3, pp. 255–270, 2011.

[88] Y. M. Dai, S. C. Tang, J. Q. Peng et al., "MnO_2@SnO_2 coreshell heterostructured nanorods for supercapacitors," *Materials Letters*, vol. 130, pp. 107–110, 2014.

[89] R. Li, X. Ren, F. Zhang, C. Du, and J. Liu, "Synthesis of Fe_3O_4@SnO_2 core-shell nanorod film and its application as a thin-film supercapacitor electrode," *Chemical Communications*, vol. 48, no. 41, pp. 5010–5012, 2012.

[90] J. Yan, E. Khoo, A. Sumboja, and P. S. Lee, "Facile coating of manganese oxide on tin oxide nanowires with high-performance capacitive behavior," *ACS Nano*, vol. 4, no. 7, pp. 4247–4255, 2010.

[91] P. Manivel, S. Ramakrishnan, N. K. Kothurkar et al., "Optical and electrochemical studies of polyaniline/SnO_2 fibrous nanocomposites," *Materials Research Bulletin*, vol. 48, no. 2, pp. 640–645, 2013.

[92] L. H. Bao, J. F. Zang, and X. D. Li, "Flexible Zn_2SnO_4/MnO_2 core/shell nanocable-carbon microfiber hybrid composites for high-performance supercapacitor electrodes," *Nano Letters*, vol. 11, no. 3, pp. 1215–1220, 2011.

[93] T. Lu, Y. Zhang, H. Li, L. Pan, Y. Li, and Z. Sun, "Electrochemical behaviors of graphene-ZnO and graphene-SnO_2 composite films for supercapacitors," *Electrochimica Acta*, vol. 55, no. 13, pp. 4170–4173, 2010.

[94] G. Arabale, D. Wagh, M. Kulkarni et al., "Enhanced supercapacitance of multiwalled carbon nanotubes functionalized with ruthenium oxide," *Chemical Physics Letters*, vol. 376, no. 1-2, pp. 207–213, 2003.

[95] B. J. Lee, S. R. Sivakkumar, J. M. Ko, J. H. Kim, S. M. Jo, and D. Y. Kim, "Carbon nanofibre/hydrous RuO_2 nanocomposite electrodes for supercapacitors," *Journal of Power Sources*, vol. 168, no. 2, pp. 546–552, 2007.

[96] D. Kalpana, K. S. Omkumar, S. S. Kumar, and N. G. Renganathan, "A novel high power symmetric ZnO/carbon aerogel composite electrode for electrochemical supercapacitor," *Electrochimica Acta*, vol. 52, no. 3, pp. 1309–1315, 2006.

[97] A. G. El-Deen, N. A. M. Barakat, K. A. Khalil, M. Motlak, and H. Y. Kim, "Graphene/SnO_2 nanocomposite as an effective electrode material for saline water desalination using capacitive deionization," *Ceramics International*, vol. 40, no. 9, pp. 14627–14634, 2014.

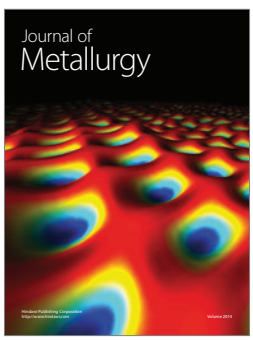

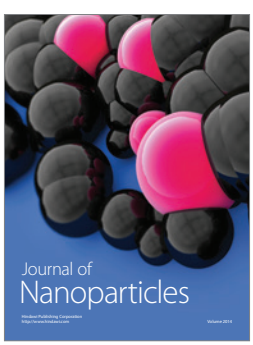

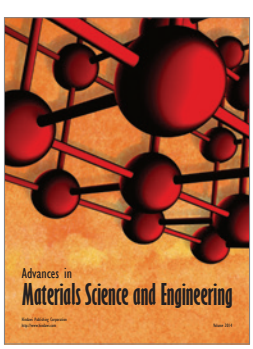

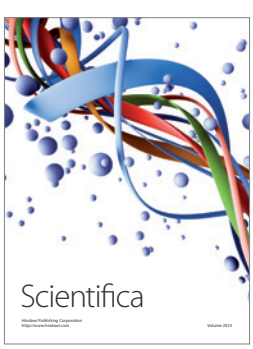

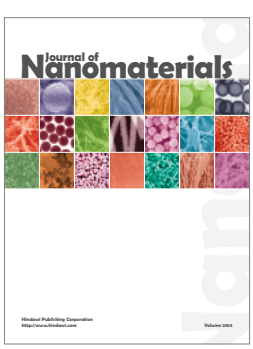

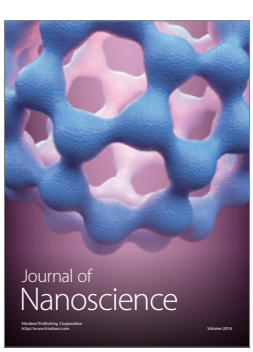

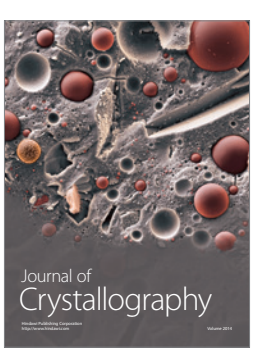

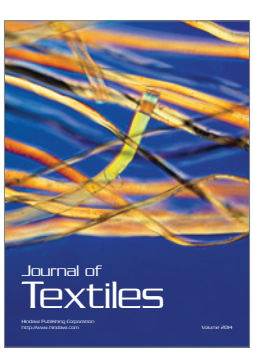

Hindawi

Submit your manuscripts at
http://www.hindawi.com